Defect-controlled binder jetting (BJT) additive manufacturing through dimensionless mapping of binder spreading and penetration

Ertiza Hossain Shopnil*

Department of Mechanical Engineering, Virginia Tech, Blacksburg, VA 24061, USA
VTMADE, Virginia Tech, Blacksburg, VA 24061, USA

Abstract

Binder jetting (BJT) a metal additive manufacturing process with broad material compatibility. The resolution of the printed parts is dependent on binder-powder interaction and the mechanisms that infiltrate binder into the powder bed during printing, and controlling the defects related to this infiltration, such as balling and bleeding. Binder spreading and penetration are dependent on capillary suction and viscous resistance of the powder bed, which are depicted by the packing density of the spread powder layer. Prior studies have only emphasized strategies to increase the powder packing density. Here, a systematic analysis of powder packing density and binder infiltration dynamics shows that neither loose packing nor tight packing is suitable for defect-free printing. Therefore, two dimensionless numbers: binder penetration number, Bp, and binder spreading number, Bs, are introduced that collapse all binder material properties, binder deposition-related process parameters, and powder properties to provide the range of powder packing density for defect-free printing. This work establishes the foundation for developing customized binders for printing new materials, expanding the material compatibility of the BJT process.

Keywords: Binder jetting (BJT); Packing density; Balling; Bleeding; Dimensionless number.
*To whom correspondence should be addressed: ertizahossain143@vt.edu

1 Introduction

Binder jetting (BJT) is a powder-based additive manufacturing (AM) process that stands out among other metal AM processes for its broad material compatibility and uniform microstructure [1]. Unlike fusion-based AM processes (i.e., powder bed fusion, direct energy deposition), BJT doesn't require continuous melting and solidification while printing, thus ensuring fabrication of parts without residual stress. Figure 1 illustrates the process workflow. A vibrating hopper spreads powder, and a counter-rotating roller compacts the powder bed, providing proper packing density. An array of nozzle deposits droplets of binder on the powder bed, followed by partial evaporation of binder solvents by a heating lamp. This process repeats layer by layer to fabricate the green part, which is cured in a curing oven, followed by depowdering. Then the green part is densified by means of high-temperature sintering.

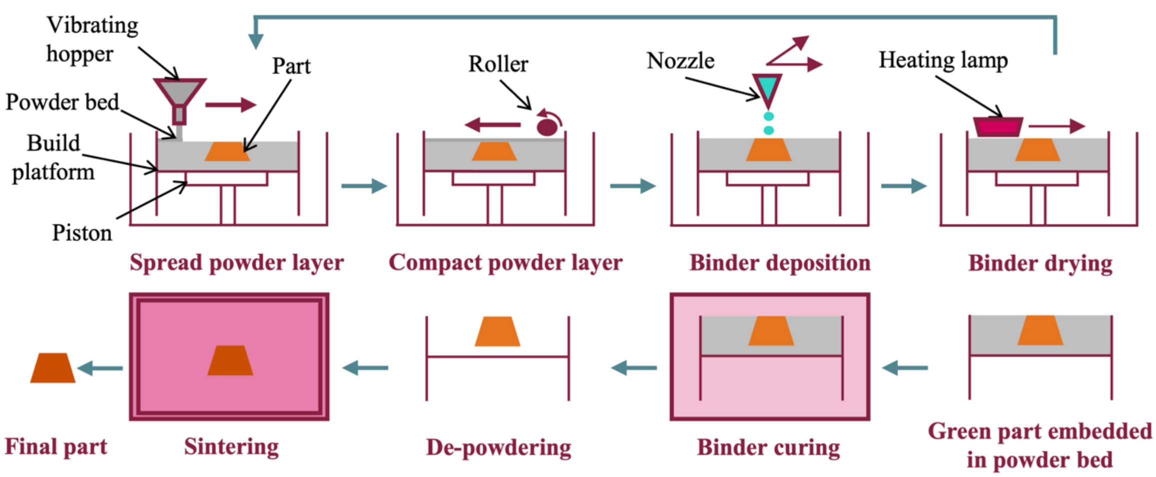

Figure 1: Process workflow of binder jetting (BJT).

Defect-free fabrication through binder jetting is depicted by the capillary-driven infiltration of binder into the porous powder bed. The viscous resistance of the porous powder bed works as a limiting factor against binder infiltration, thus keeping the binder within the intended geometry, the core requirement for high-resolution printing [2]. The capillary suction of binder droplets is depicted by the pore size of the powder bed, which is controlled by the powder packing density. Figure 2 illustrates the binder deposition and infiltration dynamics into a loose and tightly packed powder bed. Tightly packed powder bed generates high capillary suction, but it also increases the viscous resistance [3], lengthening the time for the binder to fully infiltrate, which keeps the binder droplet on the powder bed surface for a longer period, risking the excessive coalescence of subsequent deposited droplets, leading to balling defects and bulging (lateral (xy) overspreading of binder) [4]. In contrast, when the powder packing density is low, pore sizes are large, and viscous resistance and capillary suction are low. However, the binder infiltration is quick, which eliminates balling or bulging by making droplets penetrate the powder before deposition of subsequent droplets. But, due to less viscous resistance, the binder may go vertically beyond the intended geometry (bleeding). Also, a low packing density reduces the part's final density [5].

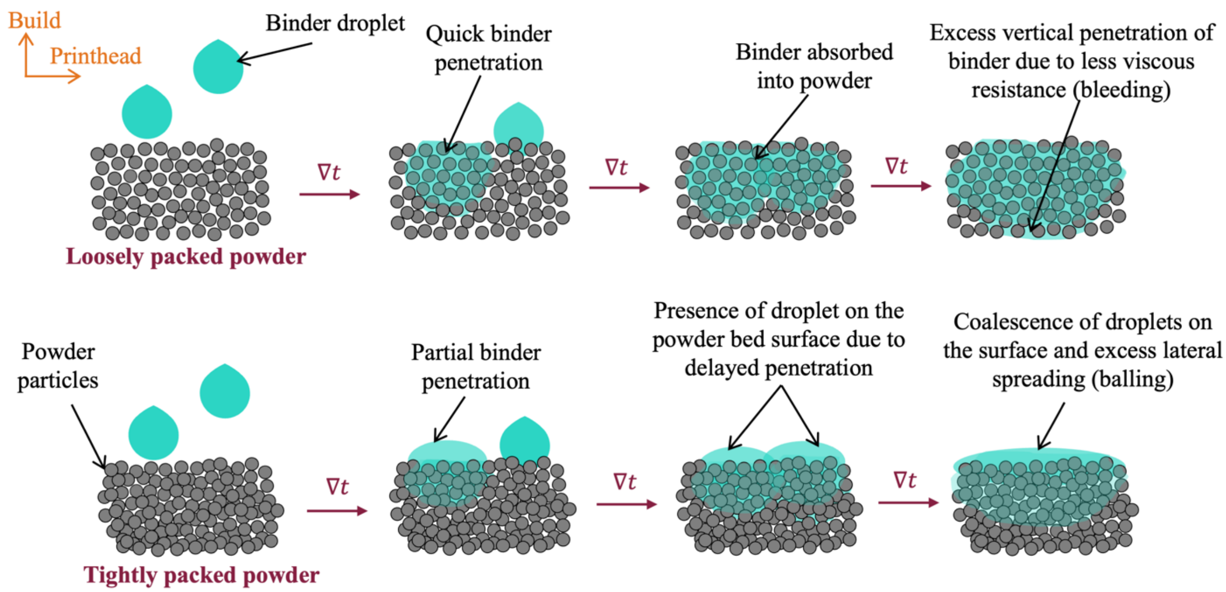

Figure 2: Binder deposition and infiltration into a loosely and a tightly packed powder bed.

The interplay between capillary suction and viscous resistance determines the occurrence of defects such as balling, bulging, and bleeding. Although prior literature emphasizes improving the powder packing density [6,7], both low and high packing densities have an impact on the binder infiltration mechanism, and a balance between the driving and resisting forces that controls this mechanism necessitates finding a sweet spot for powder packing density for a given binder and powder type for proper binder infiltration, such that balling, bulging, and bleeding are eliminated, ensuring defect-free fabrication.

Therefore, this study constructs a regime map for defect-free printing, introducing two dimensionless numbers universal for binder and feedstock type, identifying the optimal powder packing density range at which vertical infiltration by capillary suction is fast enough to prevent excess lateral spreading (balling and bulging), yet viscous resistance is high enough to arrest vertical over-penetration (bleeding).

2 Methodology

During binder deposition, the inertia of the droplets defines the initial lateral spreading, the capillary action infiltrates the binder into the powder bed, and viscous resistance limits the vertical infiltration. Variables involved in this process are: droplet diameter D_o, impact velocity U_o, binder type (density ρ, viscosity μ, surface tension γ, contact angle with the powder bed θ), feedstock powder type (particle size d_p), powder packing density φ (controlled by the roller kinematics), bed porosity ε, effective pore radius r_p, powder layer thickness h, and time interval between subsequent droplet deposition Δt. Using micro-scale binder droplets eliminates the effect of gravity.

The effective pore radius r_p, assuming the spherical powder particles (see Appendix for full derivation)

$$r_p = \frac{d_p(1-\varphi)}{3\varphi} \tag{2.1}$$

Using the Kozney-Carman (KC) [8,9] equation, the permeability k of the porous powder bed:

$$k = \frac{\varepsilon^3}{c\, S_v^{\,2}(1-\varepsilon)^2} \tag{2.2}$$

Where S_v is the specific surface area of the particle, and c is a constant, and $c = 4.8$ to 5 for spherical particles [10]. Plugging the eqn. (1), $S_v = 6/d_p$, and $c = 5$ into eqn. (2.2) gives:

$$k = \frac{d_p^{\,2}(1-\varphi)}{180\varphi^2} \tag{2.3}$$

Capillary pressure that drives the binder into the powder bed:

$$P_c = \frac{2\gamma\cos\theta}{r_p} = \frac{6\gamma\varphi\cos\theta}{d_p(1-\varphi)} \tag{2.4}$$

For a given binder type, k and P_c are $f(d_p, \varphi)$. Altering packing density or particle size has the opposite effect on the capillary pressure and the permeability.

The vertical penetration of binder into the powder at time t is given by (see Appendix for full derivation) [11]:

$$z(t) = \left(\frac{d_p\gamma(1-\varphi)\cos\theta}{15\mu\varphi}t\right)^{\frac{1}{2}} \tag{2.5}$$

For a given binder type, the penetration depth is $f(d_p, \varphi, t)$.

Lateral spreading of the binder is initially driven by the impact velocity of the droplet. If β is the spreading factor (the ratio of the maximum diameter of the droplet at the spread from to the diameter before impact) [12], then the initial spreading radius is:

$$R_i = \frac{\beta D_o}{2} \tag{2.6}$$

This radius gives the lateral resolution of the printed primitive.

The deposited binder volume must be accommodated by the pores present in the powder layer. To keep the binder inside the intended geometry, the pores present in the powder layer should provide enough room for the supplied binder. So, the required penetration depth, z_v of binder to accommodate supplied binder volume is given by (see Appendix for full derivation):

$$z_v = \frac{2D_o}{3(1-\varphi)\beta^2} \tag{2.7}$$

Equation (2.7) suggests that more lateral spreading of the droplet upon impact on the powder bed leads to less penetration depth. Also, a powder layer with high packing density has fewer pores, and to accommodate the binder volume, the required penetration depth increases.

The time required to infiltrate the whole volume of the binder droplet, t_{abs} is found by setting $z(t_{abs}) = z_v$ using eqn. (2.5) and (2.7), which gives (see Appendix for full derivation):

$$t_{abs} = \frac{20\mu\varphi D_o^{\,2}}{3d_p\gamma(1-\varphi)^3\beta^4\cos\theta} \tag{2.8}$$

Equation (2.8) suggests that higher packing density delays the binder infiltration time, whereas increasing the lateral spreading of the droplet reduces it because more binder is distributed over a larger area on the powder bed surface.

3 Results and discussion

To avoid excess lateral coalescence of droplets (i.e., balling or bulging), the binder should be infiltrated into the powder bed before the deposition of a neighboring set of droplets, meaning the following condition should be satisfied:

$$\frac{t_{abs}}{\nabla t} = \pi_t = \frac{20\mu\varphi D_o^{\,2}}{3d_p\gamma(1-\varphi)^3\beta^4\cos\theta\,\nabla t} < 1 \tag{3.1}$$

To avoid vertical overpenetration (bleeding), the binder should not penetrate deeper than the desired z height of the powder layer. The maximum allowable penetration depth, z_{max} must be equal to the layer thickness, h. The $z(t)$ must be within the z_{max} in Δt time. So, the following condition must be satisfied:

$$\frac{z(\nabla t)}{z_{max}} = \pi_z = \left(\frac{d_p\gamma\cos\theta(1-\varphi)}{15\mu\varphi h^2}\nabla t\right)^{\frac{1}{2}} < 1 \tag{3.2}$$

Introducing a dimensionless capillary time, t^*, such that:

$$t^* = \frac{\gamma}{\mu D_o}\nabla t \tag{3.3}$$

Another dimensionless length scale, x^* defined as:

$$x^* = \frac{d_p}{D_o} \tag{3.4}$$

Plugging these dimensionless time and length scales into eqn. (3.1) and (3.2) give:

$$\pi_t = \frac{20\varphi x^*}{3(1-\varphi)^3\beta^4\cos\theta\ t^*} \tag{3.5}$$

$$\pi_z = \frac{(1-\varphi)\cos\theta}{15\varphi\left(\frac{h}{D_o}\right)^2} t^* x^* \tag{3.6}$$

From eqn. (3.5) and (3.6), collapsing all the dimensionless terms into two newly introduced dimensionless numbers: binder penetration number, Bp, and binder spreading number, Bs, gives:

$$\pi_t = \frac{20\varphi}{3(1-\varphi)^3 \mathrm{Bs}} \tag{3.7}$$

$$\pi_z = \frac{Bp\,(1-\varphi)}{15\varphi} \tag{3.8}$$

Where the dimensionless numbers are:

$$\mathrm{Bs} = \frac{\cos\theta\, \beta^4 t^*}{x^*} = \frac{\cos\theta\,\left(D_{max}\right)^4 \gamma\, \nabla t}{\left(D_o\right)^4 \mu d_p} \tag{3.9}$$

$$\mathrm{Bp} = \frac{\cos\theta\ t^* x^*}{\left(\frac{h}{D_o}\right)^2} = \frac{\cos\theta\ \gamma d_p\, \nabla t}{h^2 \mu} \tag{3.10}$$

The criteria for printing without balling or bulging:

$$\mathrm{Bs} > \frac{20\varphi}{3(1-\varphi)^3} = \mathrm{Bs}_{cr} \tag{3.11}$$

And for printing without bleeding:

$$\mathrm{Bp} < \frac{15\varphi}{1-\varphi} = \mathrm{Bp}_{cr} \tag{3.12}$$

Equations (3.11) and (3.12) provide the allowable packing density based on Bs and Bp, which includes all properties related to binder and the powder particle size, and also the selected layer thickness of the powder. Figure 3 shows the critical binder penetration and spreading numbers (Bp_{cr} and Bs_{cr}) for different powder packing densities. The bleeding and balling-free printing zone is between the Bp_{cr} and Bs_{cr} curves (Fig. 3) until the point where they intersect each other, after which balling-free printing is not possible. Still, the bleeding is eliminated because of high viscous resistance.

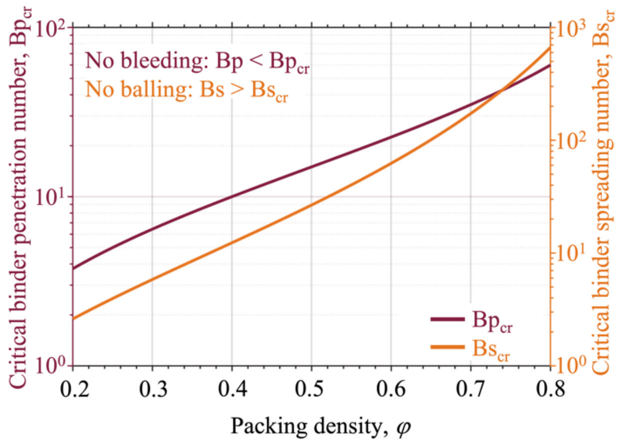

Figure 3: Critical binder penetration and spreading numbers as a function of powder packing density.

Figure 4 shows the defective and defect-free printing zones for different values of the Bp and Bs as a function of packing density. The defect-free zone depends on the Bp and Bs (i.e., binder property, selected thickness of the spread powder layer, and powder particle size). For low Bp and high Bs, the defect-free zone is wide (Fig. 4 (a)). Higher value of Bp narrows the defect-free zone (Fig 4. (b)). Lowering the Bs also narrows the defect-free zone (Fig 4. (c)). High Bp and low Bs lead to a highly defective zone where both bleeding and balling are present (Fig. 4 (d)).

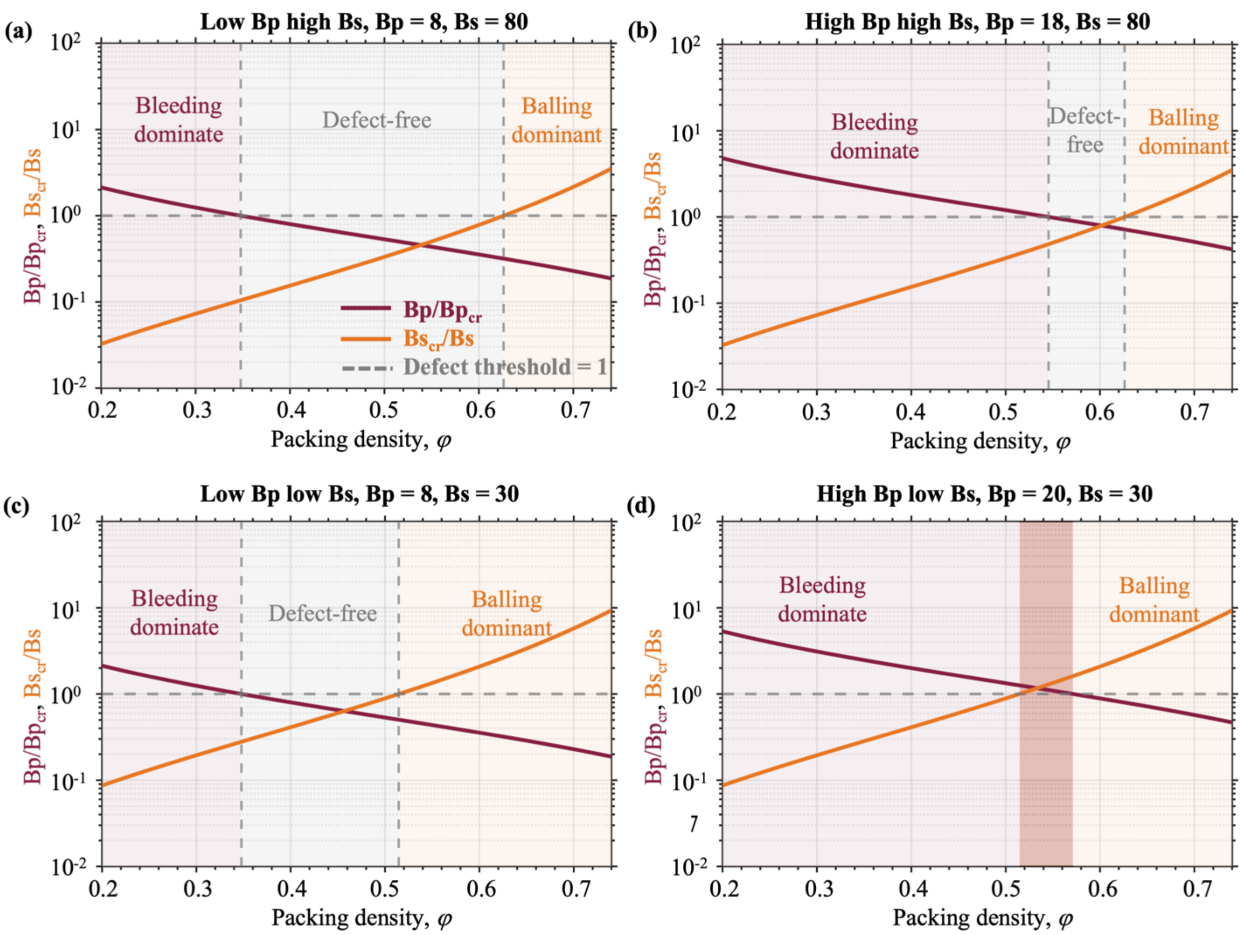

Figure 4: Ratio of Bp to Bp_{cr} and Bs_{cr} to Bs against the powder packing density, showing the defective and defect-free printing zones.

4 Conclusion

This work introduces two dimensionless numbers: binder penetration number, Bp, and binder spreading number, Bs, which are used to construct a regime map showing the defective and defect-free binder jetting (BJT) printing zones for different powder packing densities.

Lateral overspreading of binder droplets by remaining for a longer period and coalescence with subsequent binder droplets on the powder bed surface, and vertical over penetration beyond the intended geometry due to less viscous resistance of the powder bed are the sources of two defects: balling and bleeding. For a given binder and powder type, the binder penetration time and depth depend on the packing density of the powder after compaction by the roller. Too loose and too tight powder packing are prone to bleeding and balling defects, respectively. The packing density range where defect-free printing is possible is determined by collapsing all properties of the binder (viscosity, surface tension, and contact angle), binder deposition-related process parameters (droplet diameter, time interval between consequent droplet deposition from the nozzle, and droplet impact velocity), and geometric properties of powder (particle size) into dimensionless numbers Bp and Bs.

Outcomes of this work are: defect-free printing by tuning the powder packing density for a given binder and powder type, developing customized binders for a specific type of powder and the packing density by tuning the Bp and Bs, so that defect-free printing is possible, tuning process parameters (powder layer thickness, binder droplet size and velocity, consecutive droplet arrival time) for a given powder type so that the Bp and Bs fall within the defect-free printing zone, and expanding BJT printable materials without printing defects.

5 References

[1] Gibson, I., Rosen, D., and Stucker, B., 2015, *Additive Manufacturing Technologies: 3D Printing, Rapid Prototyping, and Direct Digital Manufacturing*, Springer, New York, NY. https://doi.org/10.1007/978-1-4939-2113-3.

[2] Ramalingam, M. S., Chaithanya Kumar, K. N., Sharma, S., Joshi, S. S., and Dahotre, N. B., 2025, "Binder Jet Additive Manufacturing: A Review of Modelling Approaches and Experimental Observations on Green Part Printing," Virtual Phys. Prototyp., **20**(1), p. e2547091. https://doi.org/10.1080/17452759.2025.2547091.

[3] Diener, S., Zocca, A., and Günster, J., 2021, "Literature Review: Methods for Achieving High Powder Bed Densities in Ceramic Powder Bed Based Additive Manufacturing," Open Ceram., **8**, p. 100191. https://doi.org/10.1016/j.oceram.2021.100191.

[4] Colton, T., and Crane, N. B., 2021, "Influence of Droplet Velocity, Spacing, and Inter-Arrival Time on Line Formation and Saturation in Binder Jet Additive Manufacturing," Addit. Manuf., **37**, p. 101711. https://doi.org/10.1016/j.addma.2020.101711.

[5] Chen, L., Chen, W., Zhang, S., Zou, S., Cheng, T., and Zhu, D., 2023, "Effect of Bimodal Powder on Densification and Mechanical Properties of 316L Stainless Steel Fabricated by Binder Jet 3D Printing," J. Mater. Res. Technol., **27**, pp. 4043–4052. https://doi.org/10.1016/j.jmrt.2023.10.203.

[6] Lee, Y., Nandwana, P., and Simunovic, S., 2022, "Powder Spreading, Densification, and Part Deformation in Binder Jetting Additive Manufacturing," Prog. Addit. Manuf., **7**(1), pp. 111–125. https://doi.org/10.1007/s40964-021-00214-1.

[7] Miyanaji, H., Rahman, K. M., Da, M., and Williams, C. B., 2020, "Effect of Fine Powder Particles on Quality of Binder Jetting Parts," Addit. Manuf., **36**, p. 101587. https://doi.org/10.1016/j.addma.2020.101587.

[8] Wyllie, M. R. J., and Rose, W. D., 1950, "Application of the Kozeny Equation to Consolidated Porous Media," Nature, **165**(4207), pp. 972–972. https://doi.org/10.1038/165972a0.

[9] Tiab, D., and Donaldson, E. C., 2024, *Petrophysics: Theory and Practice of Measuring Reservoir Rock and Fluid Transport Properties*, Elsevier. [Online]. Available: https://books.google.com/books?id=WOTPEAAAQBAJ.

[10] Ozgumus, T., Mobedi, M., and Ozkol, U., 2014, "Determination of Kozeny Constant Based on Porosity and Pore to Throat Size Ratio in Porous Medium with Rectangular Rods," Eng. Appl. Comput. Fluid Mech., **8**(2), pp. 308–318. https://doi.org/10.1080/19942060.2014.11015516.

[11] Govindarajan, S. K., Pavan, T. N. V., Devarapu, S. R., and Kumar, G., 2025, “Critical Review on Challenges in the Application of Darcy’s Law for Multi-Phase Fluid Flow in Petroleum Reservoirs,” Discov. Appl. Sci., **7**(3), p. 201. https://doi.org/10.1007/s42452-025-06632-y.
[12] Budakli, M., 2021, “Prediction of Maximum Spreading Factor after Drop Impact: Development of a Novel Semi-Analytical Model Incorporating Effect of Surface Roughness,” Colloid Interface Sci. Commun., **41**, p. 100384. https://doi.org/10.1016/j.colcom.2021.100384.